Conference Paper, Published Version

Kimura, Ichiro; Hosoda, Takashi; Iwata, M.

A depth averaged model of open channel flows with a horseshoe vortex

River Flow 2010 - Dittrich, Koll, Aberle & Geisenhainer (eds) - © 2010 Bundesanstalt für Wasserbau ISBN 978-3-939230-00-7

A depth averaged model of open channel flows with a horseshoe vortex

I. Kimura
Hokkaido University, Sapporo, Japan

T. Hosoda
Kyoto University, Kyoto, Japan

M. Iwata
CTI Engineering Co. Ltd., Tokyo, Japan

ABSTRACT: The depth-averaged models have a great advantage in computational efficiency compared with 3D (three-dimensional) models. If 3D flow structures are predominant, depth-averaged 2D models are not applicable. Recently, several sophisticated 2D depth-averaged model, in which some 3D flow structures, such as, secondary currents of the first kind, or the vertical acceleration are incorporated, have been proposed. However, a horseshoe vortex in front of a bluff body, which also contains a typical 3D flow feature, has not been considered into any depth-averaged models. In order to consider a horseshoe vortex in depth averaged equations, we propose a novel physical based model for a horseshoe vortex in front of a bed mounted cylinder. The model can reproduce the horseshoe vortex if the profiles of the depth and the depth-averaged velocity in the stream-wise directions are given. For model validation, the present model is applied to two kinds of flows, namely, a potential flow around a circular cylinder and 3D URANS computations of a flow around a square cylinder. The results showed that the present model can capture the fundamental features of a horseshoe vortex excellently.

Keywords: Plane 2D model, Shallow flow equations, Horseshoe vortex, Local scour

1 INTRODUCTION

Depth-averaged plane 2D (two-dimensional) shallow flow equations have been widely used for computations of various phenomena in rivers and shallow lakes. The numerical models based on the plane 2D shallow flow equations have a great advantage from the viewpoint of computational efficiency compared with 3D (three-dimensional) models. Though the computer is developing rapidly and also 3D numerical models are becoming common nowadays (e.g., Nagata et al. (2005)), the 3D computations are still expensive and not practical for engineering purposes. Generally speaking, a horizontal scale of rivers is much larger than a vertical scale. Therefore, the assumption of shallow flows is reasonable in many cases. However, the plane 2D models sometimes yield serious errors if the three-dimensionality of flows becomes conspicuous.

Secondary currents of the first kind at curved channels are typical cases of river flows with crucial three-dimensionality. The 2D depth-averaged model incorporated the effects of secondary currents of the first kind were firstly proposed by Kalkwijk & de Vriend (1980). After then, such models have been refined and extended their applicability by many researchers, such as, Hosoda et al. (2001), Onda (2004) and Onda et al. (208). Applications of the 2D models with effects of secondary current have also done widely in real river phenomena with bed deformation, such as, meandering channel (Kimura et al. (2009)) and a side-cavity with recierculation (Kimura et al. (2008)).

Another typical three-dimensional flow structure can be seen around a bluff body, such as, bridge piers, spur-dikes, etc. Those 3D structures are characterized by formations of a horseshoe vortex at upstream region of the bluff body and an arch vortex at downstream region of it. A horseshoe vortex formation is particularly important for river engineering because a horseshoe vortex is closely related to local scour erosion around a river structure, which sometimes threatens the safety of river structures. However, so far, the 2D depth averaged model considering effects of horseshoe vortex was not been proposed except some ad hoc approach.

In this paper, we developed a model of a horseshoe vortex for incorporating into depth-averaged 2D shallow open channel equations. For model

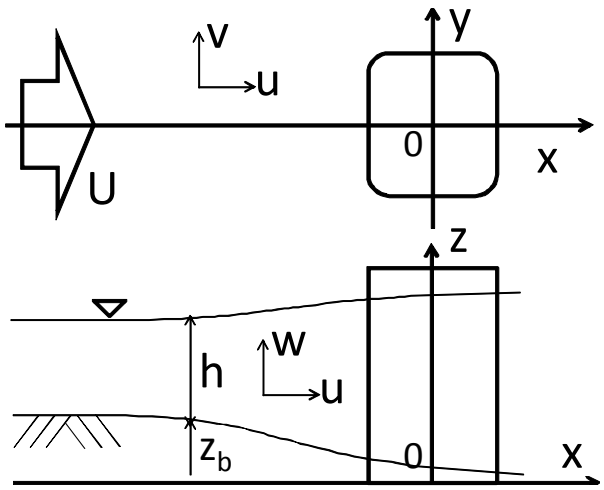

Figure 1. Schematic diagram of the flow domain.

building, velocity profiles in vertical directions are expressed as polynomials of vertical coordinate. We chose polynomial type functions considering analytical simplicity. The assumed velocity profiles are substituted into both three-dimensional and depth-averaged continuity and momentum equations. Then the relations of coefficients for each term are derived. As the first step of model development, we assumed a hydrostatic condition as well as simplified flow domain. We also chose the lowest order of polynomial functions to express a horseshoe vortex for simplicity.

The present model was verified through the comparison with two kinds of simple flow phenomena; one is a potential flow around a circular cylinder and the other is a three-dimensional numerical result of a horseshoe vortex in front of a square cylinder studied by Kimura et al. (2006). The calculated results show the validity of the present model and the applicability to real river phenomena with a horseshow vortex.

2 DERIVATION OF THE PRESENT MODEL

2.1 *Basic assumption*

We consider a flow field schematically shown in Figure 1. The flow domain is assumed as symmetric with respect to the center line (x-axis) and the lateral velocity v on the centerline is assumed to be 0. First, the three-dimensional velocity profiles in the streamwise direction (u) and the transverse direction (v) are expressed by polynomials of ζ as follows.

$$u = u(x,\zeta) = u_0(x) + u_1(x)\zeta + u_2(x)\zeta^2 + u_3(x)\zeta^3 + u_4(x)\zeta^4 + u_5(x)\zeta^5 + u_6(x)\zeta^6 + u_7(x)\zeta^7 + \cdots \quad (1)$$

$$v = v(x,\zeta) = v_0(x) + v_1(x)\zeta + v_2(x)\zeta^2 + v_3(x)\zeta^3 + v_4(x)\zeta^4 + v_5(x)\zeta^5 + v_6(x)\zeta^6 + v_7(x)\zeta^7 + \cdots \quad (2)$$

$$\zeta = \frac{z - z_b}{h} \quad (3)$$

where z: water depth, z_b: bed height and (u, v): velocities in (x, y) directions. The velocity in the vertical direction, w(x, ζ) can be expressed using the three-dimensional continuity equation:

$$\frac{\partial u}{\partial x} + \frac{\partial v}{\partial y} + \frac{\partial w}{\partial z} = 0 \quad (4)$$

and equations (1) and (2) as:

$$\begin{aligned} w = w(x,\zeta) = {} & -h\zeta\frac{\partial v_0}{\partial y} - h\frac{\zeta^2}{2}\frac{\partial v_1}{\partial y} - h\frac{\zeta^3}{3}\frac{\partial v_2}{\partial y} \\ & - h\frac{\zeta^4}{4}\frac{\partial v_3}{\partial y} - h\frac{\zeta^5}{5}\frac{\partial v_4}{\partial y} - h\frac{\zeta^6}{6}\frac{\partial v_5}{\partial y} - h\frac{\zeta^7}{7}\frac{\partial v_6}{\partial y} \\ & - h\frac{\zeta^8}{8}\frac{\partial v_7}{\partial y} - \frac{\partial h}{\partial x}\left(u_0\zeta + \frac{u_1}{2}\zeta^2 + \frac{u_2}{3}\zeta^3 + \frac{u_3}{4}\zeta^4 \right. \\ & \left. + \frac{u_4}{5}\zeta^5 + \frac{u_5}{6}\zeta^6 + \frac{u_6}{7}\zeta^7 + \frac{u_7}{8}\zeta^8\right) \\ & - h\zeta\frac{\partial u_0}{\partial x} - h\frac{\zeta^2}{2}\frac{\partial u_1}{\partial x} - h\frac{\zeta^3}{3}\frac{\partial u_2}{\partial x} - h\frac{\zeta^4}{4}\frac{\partial u_3}{\partial x} \\ & - h\frac{\zeta^5}{5}\frac{\partial u_4}{\partial x} - h\frac{\zeta^6}{6}\frac{\partial u_5}{\partial x} - h\frac{\zeta^7}{7}\frac{\partial u_6}{\partial x} - h\frac{\zeta^8}{8}\frac{\partial u_7}{\partial x} \\ & - h(u_0 + u_1\zeta + u_2\zeta^2 + u_3\zeta^3 + u_4\zeta^4 + u_5\zeta^5 \\ & + u_6\zeta^6 + u_7\zeta^7)\frac{\partial \zeta}{\partial x} \end{aligned} \quad (5)$$

The depth averaged velocity component in x and y directions, U and V are obtained through vertical integration of equations (1) and (2) as:

$$\begin{aligned} U = U(x) &= \int_0^1 u\,d\zeta \\ &= u_0 + \frac{u_1}{2} + \frac{u_2}{3} + \frac{u_3}{4} + \frac{u_4}{5} + \frac{u_5}{6} + \frac{u_6}{7} + \frac{u_7}{8} + \cdots \end{aligned} \quad (6)$$

$$\begin{aligned} V = V(x) &= \int_0^1 v\,d\zeta \\ &= v_0 + \frac{v_1}{2} + \frac{v_2}{3} + \frac{v_3}{4} + \frac{v_4}{5} + \frac{v_5}{6} + \frac{v_6}{7} + \frac{v_7}{8} + \cdots \end{aligned} \quad (7)$$

2.2 *Coefficients of velocity profile functions*

Coefficients (u_0, u_1, etc.) for velocity profile functions (equations (1) and (2)) are derived in the following way. For the sake of simplicity, we consider up to second order terms for u and only the 0-th order term for v, respectively. Therefore, necessary coefficient functions are $u_0(x)$, $u_1(x)$, $u_2(x)$ and $v_0(x)$.

First, using the depth-averaged continuity equation under steady condition:

$$\frac{\partial Uh}{\partial x}+\frac{\partial Vh}{\partial y}=0 \tag{8}$$

the following relation is derived.

$$-h\frac{\partial v_0}{\partial y}=\left(u_0+\frac{u_1}{2}+\frac{u_2}{3}\right)\frac{\partial h}{\partial x}+h\frac{\partial}{\partial x}\left(u_0+\frac{u_1}{2}+\frac{u_2}{3}\right) \tag{9}$$

The momentum equation in the x-direction along the centerline becomes:

$$u\frac{\partial u}{\partial x}+w\frac{\partial u}{\partial z}=-g\frac{\partial h}{\partial x}+\nu_t\frac{\partial^2 u}{\partial z^2} \tag{10}$$

where g: gravity acceleration and ν_t: eddy viscosity coefficient. The eddy viscosity coefficient is evaluated using the depth averaged velocity U (NOT friction velocity) as:

$$\nu_t=\beta' h\sqrt{U^2} \tag{11}$$

where β' is a model constant, which value should be chosen one order smaller than the case, in which a friction velocity is used for the velocity scale. On the other hand, the relation of a bed friction yields:

$$\nu_t\frac{\partial u}{\partial z}\bigg|_{\zeta=0}=\beta' h\sqrt{U^2}\,\frac{u_1}{h}=u_*|u_*| \tag{12}$$

where u_* is a signed friction velocity. In a similar way with the model proposed by Engelund (1974), the velocity near a bed (=u_0) is assumed to be in proportion with a friction velocity and is expressed using model constant r_* as:

$$u_0=r_* u_* \tag{13}$$

From equations (12) and (13), u_1 can be given using u_0 as:

$$u_1=\frac{u_*|u_*|}{\beta|U|}=\frac{u_0|u_0|}{\beta r_*^2|U|} \tag{14}$$

On the other hand, equation (1) is substituted into u in equation (10) and the relation of 0-th order of ζ becomes:

$$u_0\left(\frac{\partial u_0}{\partial x}-u_1\frac{1}{h}\frac{\partial z_b}{\partial x}\right)=-g\frac{\partial h}{\partial x}+\beta' h\sqrt{U^2}\cdot 2\frac{u_2}{h^2} \tag{15}$$

For simplicity, z_b=0 is assumed. Then, u_2 can be expressed using u_0 as:

$$u_2=\frac{h}{2\beta'\sqrt{U^2}}\left(u_0\frac{\partial u_0}{\partial x}+g\frac{\partial h}{\partial x}\right) \tag{16}$$

The 0-th order coefficient u_0, which is expressing a streamwise velocity at the bottom ($u|_{\zeta=0}$), can be derived as follows. An equation considering up to the second order terms of equation (6) becomes:

$$U=u_0+\frac{u_1}{2}+\frac{u_2}{3} \tag{17}$$

When both sides of equation (7) are multiplied by $6\beta'\sqrt{U^2}/h$, that becomes

$$\frac{6\beta'\sqrt{U^2}}{h}U=\frac{6\beta'\sqrt{U^2}}{h}u_0+\frac{3\beta'\sqrt{U^2}}{h}u_1+\frac{2\beta'\sqrt{U^2}}{h}u_2 \tag{18}$$

Next, u_1 and u_2 in equation (18) can be eliminated using equations (14) and (18). Considering non-negativity of depth averaged streamwise velocity U ($\sqrt{U^2}=U$) at upstream region of a structure, the following equation for u_0 is derived.

$$6\beta'\frac{U^2}{h}=6\beta'\frac{U}{h}u_0+3\frac{1}{hr_*^2}u_0|u_0|+u_0\frac{du_0}{dx}+g\frac{dh}{dx} \tag{19}$$

U and h in equation (19) are calculated using plane 2D (two-dimensional) computations.

Since only 0-th order term is considered for the lateral velocity v, v_0 is simply given as:

$$v_0=V \tag{20}$$

where V is calculated by a plane 2D computation.

From equations (14), (15), (19) and (20), all coefficient functions for velocity profiles u and v are determined. The vertical velocity w can be obtained by the following equation, which is derived using equation (5).

$$\begin{aligned} w=w(x,\zeta)=&-h\zeta\frac{\partial v_0}{\partial y}-\frac{\partial h}{\partial x}\left(u_0\zeta+\frac{u_1}{2}\zeta^2+\frac{u_2}{3}\zeta^3\right)\\ &-h\zeta\frac{\partial u_0}{\partial x}-h\frac{\zeta^2}{2}\frac{\partial u_1}{\partial x}-h\frac{\zeta^3}{3}\frac{\partial u_2}{\partial x}\\ &-h(u_0+u_1\zeta+u_2\zeta^2)\frac{\partial \zeta}{\partial x} \end{aligned} \tag{21}$$

Equation (9) is not directly used for model building but will be used later for comparison of lateral velocity gradient dv/dy with results by a three-dimensional computation.

2.3 *Computational procedure*

2.3.1 *Coupling with a plane 2D model*

A plane 2D computation considering a horseshoe vortex can be carried out in the following procedure:

Step 1: u_0 is calculated through equation (19) using U and h, which are computed by a plane 2D model. This process cannot be done analytical-

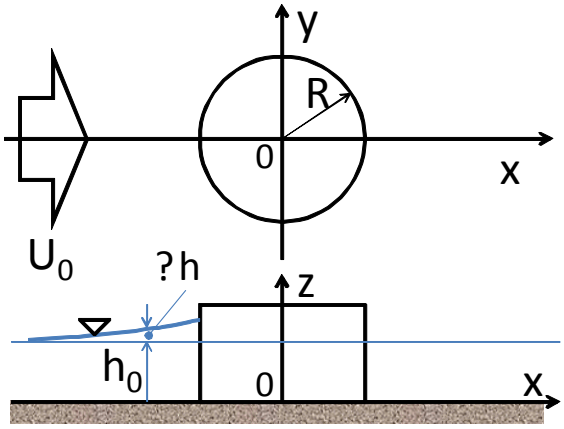

Figure 2. Schematic diagram of an open channel flow around a circular cylinder.

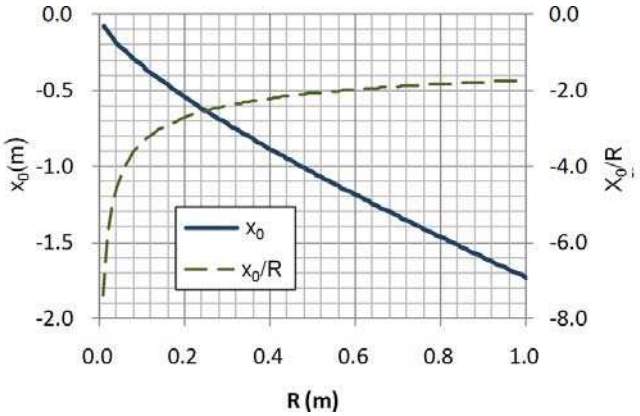

Figure 3. Relation between the diameter of the cylinder and scale of negative velocity region.

ly. So, we introduced a quasi-unsteady term du_0/dt and solved until well-developed steady state by a time marching method. An upwind scheme is applied for the third term at right hand side of equation (19) for stabilizing the time integration.

Step 2: u_1 and u_2 are calculated using equations (14) and (16) with u_0, which is obtained in Step 1.

Step 3: Using u_0, u_1, u_2 and equation (20), the vertical velocity w is calculated by equation (21).

Step 4: Depth averaged velocities U, V and a water depth h are computed by shallow flow equations, in which the bed friction is evaluated with u_*. u_* is calculated from u_0 by equation (13).

Repeating step 1 – Step 4, we can compute velocity field considering a horseshoe vortex. If the plane 2D model is coupled with sediment transport model and bed continuity equation, a local scour due to the horseshoe vortex can be computed. When the computation of 3D velocity field is not necessary, we can skip step 2 and step 3.

2.3.2 *Evaluating water elevation around a bluff body*

Another application of the present model is evaluating water elevation around a river structure using depth averaged velocities U and V. In this case, the following depth averaged momentum equation along x-axis is used.

$$\frac{\partial}{\partial x}\int_{z_b}^{z_s}\frac{u^2}{2}dz = -gh\frac{\partial h}{\partial x} - \frac{\tau_{bx}}{\rho} \tag{22}$$

$$\frac{\tau_{bx}}{\rho} = u_*|u_*| \tag{23}$$

When second orderly extended u is substituted into equation (22), the following relation:

$$h^2 + \frac{1}{g}\left(u_0^{\,2} + u_0u_1 + \frac{u_1^{\,2} + 2u_0u_2}{3} + \frac{u_1u_2}{2} + \frac{u_2^{\,2}}{5}\right)h - \left[h^2 + \frac{1}{g}\left(u_0^{\,2} + u_0u_1 + \frac{u_1^{\,2} + 2u_0u_2}{3} + \frac{u_1u_2}{2} + \frac{u_2^{\,2}}{5}\right)h\right]_{x=x_0} + \frac{2\beta'}{g}\int_{x_0}^{x} u_0\sqrt{U^2}dx = 0 \tag{24}$$

is obtained. Equations (24), (19), (14) and (16) are solved simultaneously and the depth can be estimated.

3 APPLICATION TO A POTENTIAL FLOW AROUND A CIRCULAR CYLINDER

3.1 *Flow characteristics*

In order to check the fundamental features of the present model for replicating a horseshoe vortex, an application to an open channel flow around a circular cylinder is firstly considered. The depth averaged velocities and water depth distribution around a cylinder are evaluated by a theoretical potential flow for simplicity. Figure 2 shows the plane and vertical views of the flow domain. The origin of the axes is located at the center of the cylinder on the bottom and R denotes the radius of the cylinder. U_0 and h_0 denote the velocity in x-direction and the depth at infinitely far from the cylinder, respectively. Δh denotes the water elevation around the cylinder. The bed slope is set to be 0. The theoretical solutions can be obtained analytically for U, h and Δh as follows.

$$U = U_0\left(1 - \frac{R^2}{x^2}\right) \tag{25}$$

$$h = h_0 + \Delta h \tag{26}$$

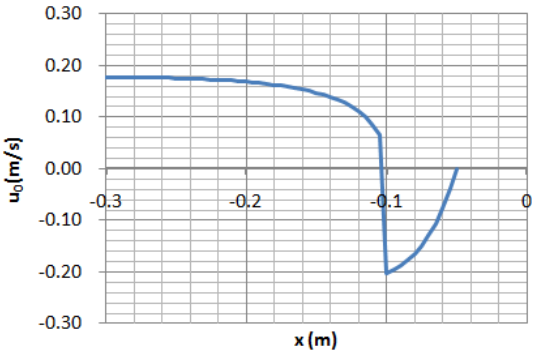

Figure 4. Predicted velocity profile (=u_0) at the bed at upstream region of the circular cylinder.

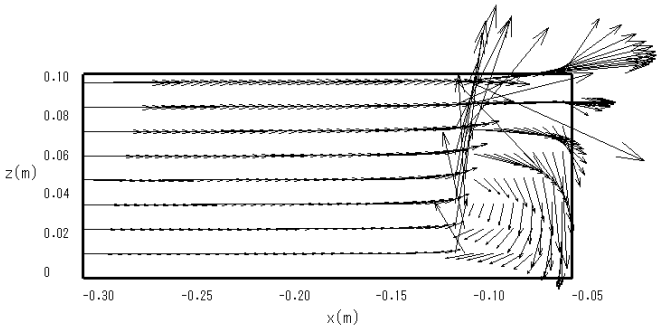

Figure 5. Velocity vectors at a vertical section along the center-line (x-axis) at the upstream regions of the cylinder.

$$\Delta h = \frac{U_0^2}{2g}\left(\frac{2R^2}{x^2} - \frac{R^4}{x^4}\right) \tag{27}$$

From those equations, the water surface slope in x-direction is calculated by

$$\frac{\partial \Delta h}{\partial x} = \frac{U_0^2}{2g}\left(-4R^2\frac{1}{x^3} + 4R^4\frac{1}{x^5}\right) \tag{28}$$

3.2 *Results and discussions*

3.2.1 *Location of the separation point*

The separation point $x=x_0$ of the horseshoe vortex at the bottom is defined as the x location of $u_0=0$, ($u|_{\zeta=0} = u_0$). This value is important for determining the horizontal scale of the horseshoe vortex.

Substituting equations (25)-(28) into equation (19), the following equation is obtained.

$$6\beta' {U_0}^2\left(1-2\frac{R^2}{x^2}+\frac{R^4}{x^4}\right) = 6\beta' U_0\left(1-\frac{R^2}{x^2}\right)u_0 + 3\frac{|u_0|u_0}{{r_*}^2} + u_0\frac{du_0}{dx}\left\{h_0 + \frac{U_0^2}{2g}\left(\frac{2R^2}{x^2}-\frac{R^4}{x^4}\right)\right\} + 2U_0^2\left\{h_0 + \frac{U_0^2}{2g}\left(\frac{2R^2}{x^2}-\frac{R^4}{x^4}\right)\right\}\left(-\frac{R^2}{x^3}+\frac{R^4}{x^5}\right) \tag{29}$$

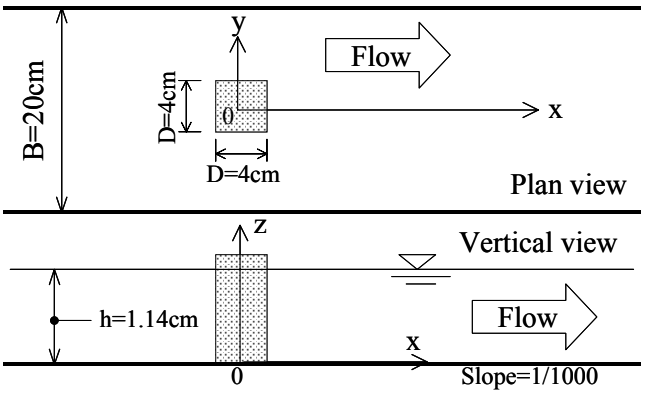

Figure 6. Schematic diagram of plan and vertical views of open channel flow around a square cylinder (Kimura et al. (2006)).

Table 1. Hydraulic parameters in 3D computation (Kimura et al. (2006).

h(cm)	U_0(cm/s)	D(cm)	B/D	h/D	Re	Fr
1.14	18.18	4.0	5	0.285	8400	0.54

h: depth, U_0: mean velocity, D: side -length of cylinder B: channel width, Re: Reynolds number (=U_0D/ξ), Fr: Froude number

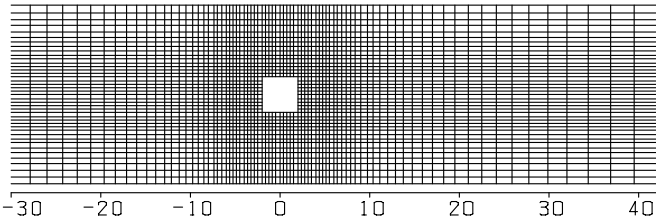

Figure 7. Computational grid used for 3D computation (Kimura et al. (2006).

When u_0 is set 0 in equation above, the following relation for x_0 is derived.

$$3\beta'\left(1-2\frac{R^2}{{x_0}^2}+\frac{R^4}{{x_0}^4}\right) = \left(-\frac{R^2}{{x_0}^3}+\frac{R^4}{{x_0}^5}\right)\left\{h_0 + \frac{U_0^2}{2g}\left(\frac{2R^2}{{x_0}^2}-\frac{R^4}{{x_0}^4}\right)\right\} \tag{30}$$

The x_0 can be calculated by solving equation (30) with iteration.

Figure 3 shows the relation of x_0 and x_0/R with different R. This figure shows that the horizontal scale of the horseshoe vortex becomes larger as R becomes larger. This feature is in compatible with real phenomena.

3.2.2 *Analytical solution for velocity field by the present model*

$u_0(x)$ is extended as a polynomial of R/x as:

$$u_0 = A_0 + A_1\frac{R}{x} + A_2\left(\frac{R}{x}\right)^2 + A_3\left(\frac{R}{x}\right)^3 + A_4\left(\frac{R}{x}\right)^4 + A_5\left(\frac{R}{x}\right)^5 + A_6\left(\frac{R}{x}\right)^6 + A_7\left(\frac{R}{x}\right)^7 + \cdots\cdots \tag{31}$$

Equation (31) is substituted into equation (29) and relations for each order are obtained. The coefficients for equation (31) were solved up to 5th order terms as follows.

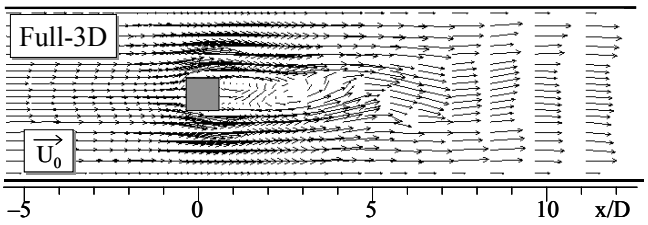

Figure 8. Snap shot of the plan flow pattern by the 3D computation (3D-DP) (Kimura et al. (2006)).

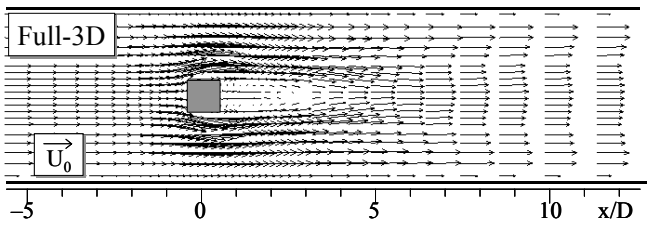

Figure 9. Time mean plane flow pattern by the 3D computation (3D-DP).

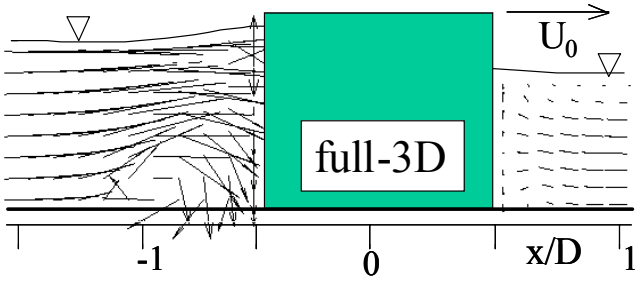

(a)3D-DP (considering dynamic pressure)

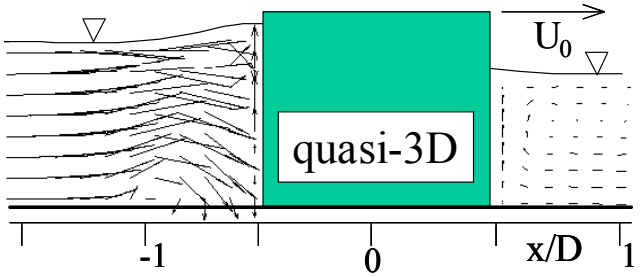

(b) 3D-SP (hydrostatic assumption)

Figure 10. Time-mean flow patterns by 3D computations at a vertical section along x-axis (Kimura et al. (2006)).

$$A_0 = r_*^2\beta' U_0\left\{1 \pm \sqrt{1 - \frac{2}{\beta' r_*^2}}\right\} \tag{32}$$

$$A_1 = 0 \tag{33}$$

$$A_3 = \frac{1}{3}\frac{h_0}{R}\frac{A_0A_2 + {U_0}^2}{\beta' U_0 - \frac{1}{r_*^2}A_0} \tag{34}$$

$$A_4 = \frac{1}{2}\frac{2\beta' U_0^2 + 2\beta' U_0 A_2 + \frac{1}{r_*^2}A_2^2 + h_0\frac{A_0A_3}{R}}{\beta' U_0 - \frac{1}{r_*^2}A_0} \tag{35}$$

$$A_5 = \frac{3\beta' U_0 A_3 - A_2A_3 + \frac{h_0}{R}(2A_0A_4 + A_2^2) + \frac{U_0^2}{gR}A_0A_2 + \frac{U_0^4}{gR} - \frac{U_0^2h_0}{R}}{3\beta' U_0 + A_0} \tag{36}$$

u_1 and u_2 can be calculated using u_0 with equations (31)-(36), equations (14) and (16).

Figure 4 shows the profile of bed velocity u_0 along x-axis when U_0 = 0.3m/s, h_0 = 0.1m/s, β' = 0.01, R = 0.05 m and r_* = 15. The region with negative u_0 shows the range of the horseshoe vortex. Figure 5 shows velocity vectors at the vertical section along x-axis. We can see a clear horseshoe vortex formation behind the cylinder. However, the present result shows unreasonable large velocity near the water surface. This feature does not agree with the real phenomena. The reason seems to be that velocity function (equation (1)) currently include only up to the second order term. Therefore, it is shown that a higher order model is necessary for improvement of the accuracy.

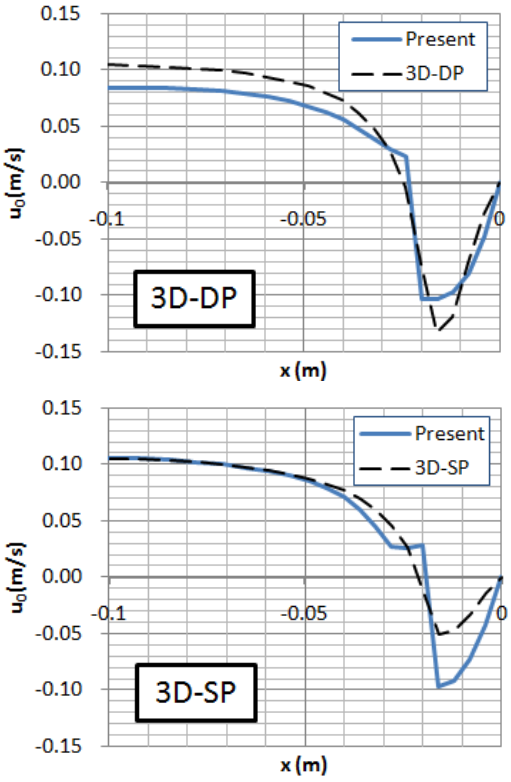

Figure 11. Predicted velocity profiles at the bed around a square cylinder by the present model (upper: 3D-DP, lower: 3D-SP).

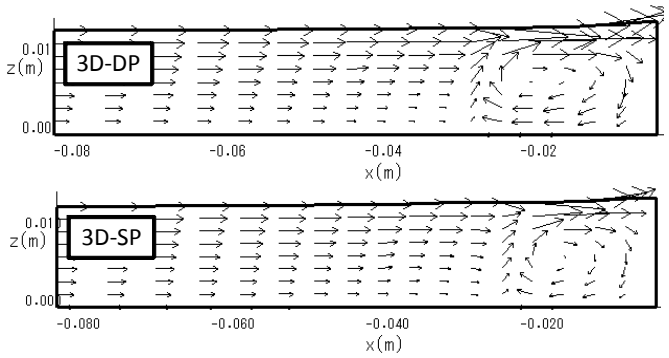

Figure 12. Predicted velocity vectors at a vertical section along x-axis by the present model (upper: 3D-DP, lower: 3D-SP).

4 COMPARISON WITH 3D URANS COMPUTATIONAL RESULTS AROUND A SQUARE CYLINDER

4.1 *Flow characteristics*

Kimura et al (2006) performed three-dimensional (3D) computations around a square cylinder mounted on a flat bed in an open channel flow using URANS (a second order non-linear k-ε model) approach. Although this study mainly focused on the backwater elevation, a horseshoe vortex was also clearly captured by the computation. Therefore, the comparison with the data is useful to check the more detailed performance of the present model.

Figure 6 shows the plane and vertical views of the tested flow domain. The hydraulic parameters used in the 3D computation are listed in Table 1. The plan view of the computational grid around the square cylinder is shown in Figure 7. Number of grid layers in the vertical direction is 8. As a turbulence model, the second order non-linear k-*e* model developed by Kimura & Hosoda (2003) was adopted. Two kinds of computations, i.e., a computation under hydrostatic assumption (case 3D-SP) and a computation considering dynamic pressure (case 3D-DP) were carried out. They also performed a plane 2D computation with depth-averaged shallow flow equations.

Figure 8 shows the instantaneous horizontal velocity vectors at the water surface by the 3D computation (case 3D-DP). We can see that Karman vortex shedding is captured numerically. It is likely that the horseshoe vortex is affected by the Karman vortex shedding and fluctuates periodically. However, the numerical result showed that the temporal velocity variation caused by the periodic Karman vortex shedding is much smaller than the mean velocity. Therefore, we use time-averaged velocities and depth of the 3D computation for validation of the present model. Figure 9 shows the time mean plane flow pattern by the 3D computation with 3D-DP. The flow field is completely symmetric to the *x*-axis.

Figure 10 shows the flow pattern in a vertical section along *x*-axis. Both computational results could capture the generation of the horseshoe vortex though the scale of the computed vortex by 3D-SP is smaller than the result by 3D-DP. As for the backwater elevation at the upstream region of the cylinder, the computation with 3D-DP could reproduced the elevation precisely though the computation with 3D-SP a little bit under-predicted it.

4.2 *Results by the present model*

4.2.1 *Outline of the model validation*

Since the present model adopts hydrostatic assumption, the model is applied to both 3D-DP and 3D-SP and results are compared. First, the depth averaged velocity *U* and *V* are calculated from the 3D numerical results through vertical integration. Using the *U*, *V* and *h* by the 3D computation, the vertical velocity profile along *x*-axis is reconstructed by the present model. Then, the vertical velocity profile along *x*-axis by the 3D computation and the present model is compared.

4.2.2 *Comparison of velocity near bed (u_0)*

Figure 11 shows the comparison of the streamwise velocity at the bed (u_0) along x-axis obtained by the 3D computation and the present model. The both results show the region where the streamsie velocity at the bed becomes negative at the upstream region of the cylinder. The profile by the present model is however not smooth contrary to the 3D computational result. This may be because of the low order approximation for u and v. Currently, the orders of velocity function is 2 for the streamwise velocity and 0 for the lateral velocity. So, we should develop a refined model with higher order approximation. As for the result by 3D-DP, the scale of the horseshoe vortex and the profile of negative velocity are in good agreement with the 3D computational result though the velocity at upstream region of the horseshoe vortex is under-predicted by the present model. On the other hand, the computation with 3D-SP could capture the scale of the horseshoe vortex though the minimum velocity is under-predicted.

In general, the present model could replicate the fundamental features of the horseshoe vortex around a square cylinder in an open channel flow. Since the present model adopted the hydrostatic assumption, it is expected that the result agrees better with 3D-SP than 3D-DP. However, such tendency was not found. The reason is also likely to be very low order approximation of velocity functions.

4.2.3 *Shape of the horseshoe vortex*

Figure 12 shows the flow pattern at the vertical section along x-axis by the present model. A horseshoe vortex is generated in both cases. The comparison with the 3D computational results reveals the difference of the shape of the horseshoe vortex clearly. In the 3D computational result, the horseshoe vortex occurs near the bottom and the shape is ellipsoidal with a longer horizontal axis. On the other hand, the range of the horseshoe vortex reaches near the surface in the result by the present model. The necessity to consider higher order terms were again shown here.

4.2.4 *Lateral velocity gradient*

The present model assumes symmetry of the flow domain. Therefore, the lateral velocity v at the centerline is always zero though the velocity gradient dv/dy is generally not zero. Figure 13 shows the value of dv/dy computed from equation (9). The result by the 3D computation is shown together. This figure shows that the results by the present model are again in good agreement with the 3D computational results in both 3D-DP and 3D-SP.

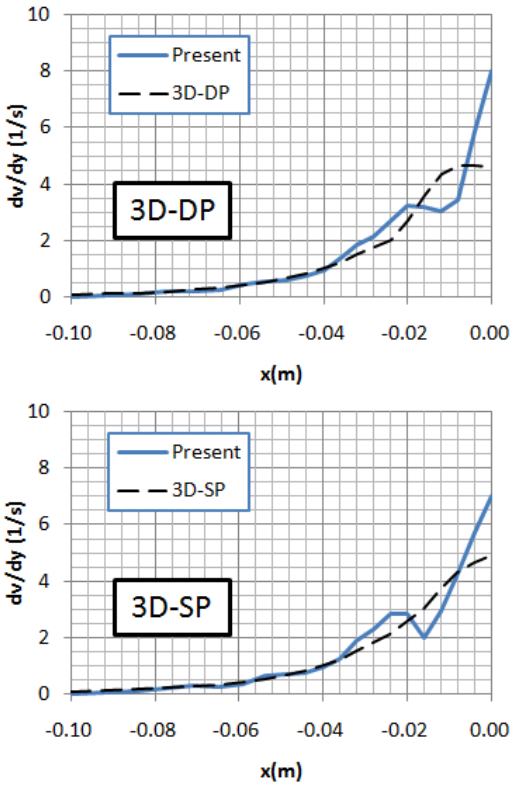

Figure 13. Predicted lateral velocity gradient dv/dy along x-axis by the present model (upper: 3D-DP, lower: 3D-SP).

5 CONCLUDING REMARKS

This study presents a novel modeling approach for a horseshoe vortex in an open channel flow for depth-averaged shallow flow equations. The present model is a first step for practical model and is imposed some restrictive assumptions, such as, symmetric flow field and flat non-sloped bed, etc. The order of approximation for velocity profiles is currently very low (second order for streamwise velocity and 0-th order for lateral velocity). The present model was applied to the potential flow around a circular cylinder and a open channel flow around a square cylinder with existing 3D URANS computational data.

The computational results indicate that the present model can replicate the horseshoe vortex formation. The range of negative velocity at the bottom and the lateral velocity gradient along the center line were also simulated adequately. However, the shape of the horseshoe vortex does not agree with the 3D computational result.

In the next step, we should modify the model in the following way.

- Considering vertical acceleration
- Increasing the order of velocity profile functions
- Extending to generalized curvilinear coordinate

ACKNOWLEDGEMENTS

Authors express their sincere thanks to Prof. Yasuyuki Shimizu (Hokkaido University) and Dr. Shinichiro Onda (Kyoto University) for their kind and fruitful advises.

REFERENCES

Engelund, F. 1974: Flow and bed topography in channel bends, *Proc. ASCE*, 100, HY11, 1631-1648.

Hosoda, T., Nagata, N., Kimura, I., Michibata, K. & Iwata, M. 2001: A depth averaged model of open channel flows with lag between main flows and secondary currents in a generalized curvilinear coordinate system. *Advances in Fluid Modeling & Turbulence Measurements, (eds. H. Ninokata, A.Wada and N. Tanaka),* World Scientific, 63-70.

Kalkwijk, J. P. & de Vriend, H. J. 1980: Computation of the flow in shallow river bends, *J. Hydraulic Res., IAHR*, 18(4), 327-342.

Kimura, I. & Hosoda, T. 2003: A non-linear k-ε model with realizability for prediction of flows around bluff bodies, *Int. J. for Numerical Methods in Fluids,* Willey, 42, 813-837.

Kimura, I., Hosoda, T. & Onda, S. 2006: Predictions of turbulent flows around a bridge pier using various numerical models, River Flow 2006, Lisbon, Portugal, Balkema, 1, 767-775.

Kimura, I., Hosoda, T. & Onda, S. 2008: Computations of suspended sediment in a shallow side-cavity using depth-averaged 2D models with effects of secondary currents, *Proc. of 2nd International Symposium on Shallow Flows*, Hong Kong, A0129, 1-6.

Nagata, N., Hosoda, T., Nakato, T. & Muramoto, Y. 2005: Three-dimensional numerical model for flow and bed deformation around river hydraulic structures, *J. Hydraulic Eng., ASCE*, 131, 1074-1087.

Onda, S. 2004: PhD Thesis, Kyoto University (in Japanese).

Onda, S., Hosoda, T. and Kimura I. 2008: Refinement of a depth averaged flow model in curved channel in generalized curvilinear coordinate system, Proc. ICHE-2008, Nagoya, Japan.